

NANO EXPRESS

Open Access



A Polarization-Dependent Normal Incident Quantum Cascade Detector Enhanced Via Metamaterial Resonators

Lei Wang, Shen-Qiang Zhai*, Feng-Jiao Wang, Jun-Qi Liu, Shu-Man Liu, Ning Zhuo, Chuan-Jin Zhang, Li-Jun Wang, Feng-Qi Liu* and Zhan-Guo Wang

Abstract

The design, fabrication, and characterization of a polarization-dependent normal incident quantum cascade detector coupled via complementary split-ring metamaterial resonators in the infrared regime are presented. The metamaterial structure is designed through three-dimensional finite-difference time-domain method and fabricated on the top metal contact, which forms a double-metal waveguide together with the metallic ground plane. With normal incidence, significant enhancements of photocurrent response are obtained at the metamaterial resonances compared with the 45° polished edge coupling device. The photocurrent response enhancements exhibit clearly polarization dependence, and the largest response enhancement factor of 165% is gained for the incident light polarized parallel to the split-ring gap.

Keywords: Infrared, Photodetectors, Polarization-selective devices, Metamaterials

Background

High-performance infrared photodetectors operating in the range of 3–14 μm are highly needed for a variety of applications, such as security surveillance, chemical sensing, and industrial process monitoring [1]. This has promoted increasing research interest in new materials and structures to improve detector performances, such as spectral sensitivity, leakage current level, and operating temperature. Thereinto, semi-conductor intersubband photodetectors have been widely explored due to their capabilities of flexible energy-band tailoring and ultrahigh-speed operation [2, 3]. Inspired by the prototype of quantum cascade laser, a new type of semi-conductor intersubband detectors, quantum cascade detectors (QCDs) have been proposed and gained great progresses over the past decade [4]. Based on bound-to-bound intersubband transitions in a built-in asymmetric conduction band structure, QCDs share the advantages of operation wavelength

designability, low noise photovoltaic operation mode and therefore room temperature operation capability over well-established detector types [5]. Thus, QCDs are largely free from the limit of the integration time due to capacitance saturation of the read-out circuit and very promising for thermal imaging. Moreover, the thermal load is strongly reduced which is of interest if the available cooling is limited, for example in spaceborne systems.[6] Up to the present, QCDs have covered a large wavelength range from the near-infrared to the terahertz region [7–14]. Many new structure designs have been presented to improved device performances, such as mini-band [12] and energy mini-steps [13] transport designs for very long wave detection and diagonal transition design [15, 16] for an improved overall performance. In addition, QCDs have prove their high-temperature operation capability [9, 17, 18], and exhibited their potential to be used for arrays in imaging applications [19].

However, QCDs suffer from the disadvantage of insensibility to normal incident light and low quantum efficiency, due to their intersubband transition principle [20]. Thus, many novel coupled structures have been applied to fulfill the intersubband transition selection rule and enhance quantum efficiency [21, 22]. Metamaterials

* Correspondence: zsqzsmbj@semi.ac.cn; fqliu@semi.ac.cn
Key Laboratory of Semiconductor Materials Science, Institute of Semiconductors, Chinese Academy of Sciences, University of Chinese Academy of Sciences; Beijing Key Laboratory of Low Dimensional Semiconductor Materials and Devices, P.O. Box 912, Beijing 100083, People's Republic of China

are man-made structures compositing of sub-wavelength periodically arranged metallic resonators that allow for three-dimensional control of light [23]. Utilization of resonant inclusions allows for the realization of stunning optical properties that cannot be found otherwise in nature, such as superlensing, negative refraction, or cloaking. These exotic properties strongly depend on the geometry of metamaterial molecules rather than their composition. Since they were theoretically proposed by Pendry et al. [24] and experimentally demonstrated by Smith et al. [25], metamaterials have attracted intensive research interest and extended to infrared region [26, 27] in recent years because of their wide applications in super lenses, slow light, data storage, optical switching, and so on. Another property of interest is that metamaterial resonators can excite a strong field enhancement in the near-field and be used as highly sub-wavelength electromagnetic cavities [28]. This property makes them the ideal candidates for coupling incoming light to a semiconductor medium and thus a promising method to enhance absorption in semi-conductor intersubband photodetectors. A. Benz et al. have innovatively applied a complementary split-ring resonator (CSRR) on a quantum-cascade-laser structure to enhanced photovoltaic detection in terahertz region and brought in inspiring results [29]. In this work, a similar structure is integrated on a quantum cascade detector in infrared region to enhance device response and, in further, the polarization selective enhancement property of the integrated device has

been focused on. The metamaterial structure is designed through three-dimensional finite-difference time-domain (FDTD) method and directly fabricated into the top metal contact, which forms a double-metal waveguide together with the metallic ground plane. For one thing, the metamaterial layer will transfer the energy of the normal incident light into metamaterial resonant modes, which will be confined in the detector active region by the double-metal waveguide, as the same in Ref. 28. For another, the integrated device is expected to exhibit clearly polarization-dependent property due to the asymmetry of the metamaterial resonators. With normal incidence, significant enhancements of photocurrent response are obtained at the metamaterial resonances compared with the 45° edge facet coupling device. The photocurrent response enhancements exhibit clearly polarization dependence, and the largest response enhancement factor of 165% is gained for the incident light polarized parallel to the splitting gap.

Methods

The quantum cascade detector used in this device was grown on a semi-insulating InP substrate by molecular beam epitaxy and designed to operate at a wavelength of $10.5\ \mu\text{m}$. The quantum cascade detector structure of one period is demonstrated in the inset of Fig. 1b in detail. The structure is a normal design, which is not well-designed for coupling with the metamaterial structure. The integrated device structure and the basic building

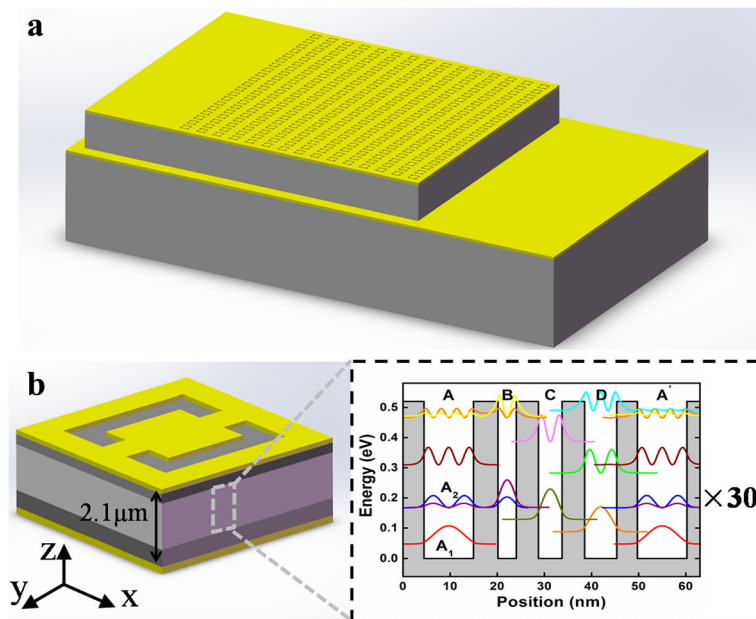


Fig. 1 **a** Schematic of the metamaterial coupled detector. **b** Three-dimensional diagram for one metamaterial building block. Inset: self-consistently calculated conduction band structure of one period of the QCD. Starting with quantum well A from left to right, the layer thicknesses in angstroms are 105/52/39/47/50/48/68/44, where $\text{In}_{0.53}\text{Ga}_{0.47}\text{As}$ wells are in *bold*, $\text{In}_{0.52}\text{Al}_{0.48}\text{As}$ barriers are in *roman*, and the *underlined* active well A is Si-doped ($n = 4.5 \times 10^{17}\ \text{cm}^{-3}$)

block of the metamaterial are described schematically in Fig. 1. A 30-period chirped InGaAs/InAlAs superlattice (SL) active region and two Si-doped InGaAs($5 \times 10^{17} \text{ cm}^{-3}$) contact layers of 500 and 200 nm are sandwiched between an upper Au metamaterial layer and a bottom Au reflection layer whose thicknesses are both 100 nm. Thus, a double-metal waveguide structure is constituted to ensure a high overlap between the active detector region and the resonant mode excited by the metamaterial. Each building block of the metamaterial consists of a CSRR, which is directly fabricated into the top metal contact layer. Figure 1b also defines the coordinate system and shows the direction of the fundamental axes, which will be used throughout this work.

The metamaterial properties, such as positions and line widths of the resonances, highly depend on the shape and size of the metallic resonators and can be fully controlled by the geometry of the resonant elements. In this work, higher order resonant modes of a complementary split-ring metamaterial are excited to interact with the intersubband transitions in the quantum cascade detector's active origin. Three-dimensional FDTD simulations are performed for the structure design. Due to the Au film on the back, the structure does not allow light transmission, and therefore, its reflectance spectra is studied to characterize the metamaterial properties. The dips in the reflectance spectra correspond to the high metamaterial absorption and thus are the metamaterial resonances. According to the response spectrum obtained from the 45° edge facet coupling device, the dimensions of the metamaterial building block are determined and illustrated in the inset of Fig. 2. Due to the asymmetry in x - y plane, the CSRRs will have different resonate properties for the incoming light with different polarized directions. Figure 2 shows the simulated reflectance spectra for two polarization incident light,

along with the response spectrum of the origin quantum cascade detector. Resonance wavelengths of 10.7 and 10.3 μm are gained for E_x and E_y polarization incident light, respectively, by geometric scaling of the CSRRs to overlap with the detector's origin response spectrum with peak wavelength of 10.5 μm . In addition, there is another resonance at 11.5 μm on the edge of the response spectrum for E_x polarization, which will have similar coupled property as the resonance at 10.7 μm . To reveal the coupling mechanism in the integrated device, the E_z electric component distributions for the structure have been simulated and shown in Fig. 3. Figure 3a, b is E_z electric component distribution in x - y plane 200 nm below the metamaterial layer inside the semi-conductor for E_x polarization incident light at 10.7 μm and E_y polarization at 10.3 μm , respectively. The different spatial mode profiles for the E_x and E_y polarization incident light indicate that our device response goes beyond a simple grating coupler which would have the same response for both polarizations. Figure 3c, d is E_z electric component distributions in x - y and y - z planes at $y=0$ and $x=0$ for E_x polarization at 10.7 μm and for E_y polarization at 10.3 μm , respectively. They demonstrate the existence of strong E_z electric component through the whole active region confirming the significant confinements by the double-metal waveguide, which is vital for the device response enhancement.

The device processing starts with the upside down mounting of the epitaxy wafer. After the deposition of a Ti(20 nm)/Au(100 nm) layer on the top contact layer, the epitaxial layer is fixed onto an InP receptor substrate using Deamcheas electricity conductive adhesive. Therefore, the Ti/Au layer deposited on the top contact layer will act as the reflection layer and bottom electrode in the integrated device. Following that, lapping and selective wet chemical etching using hydrochloric acid were

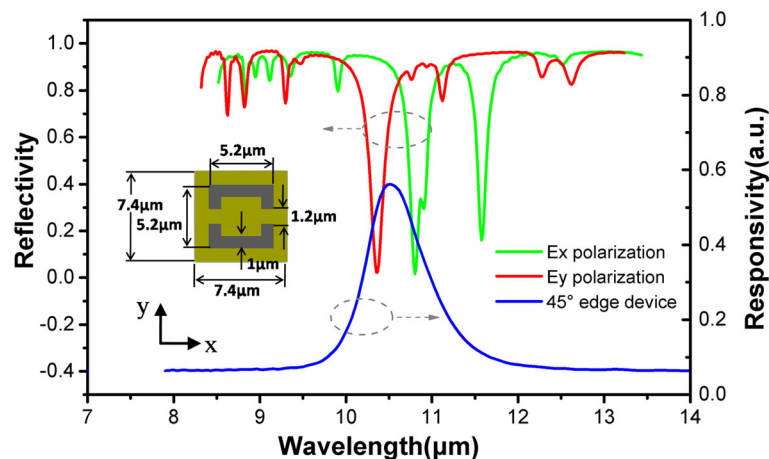


Fig. 2 Simulated reflectance spectra for E_x and E_y polarization incident light, along with the detector's origin response spectrum. Inset: the dimensions of the metamaterial structure obtained from FDTD simulation

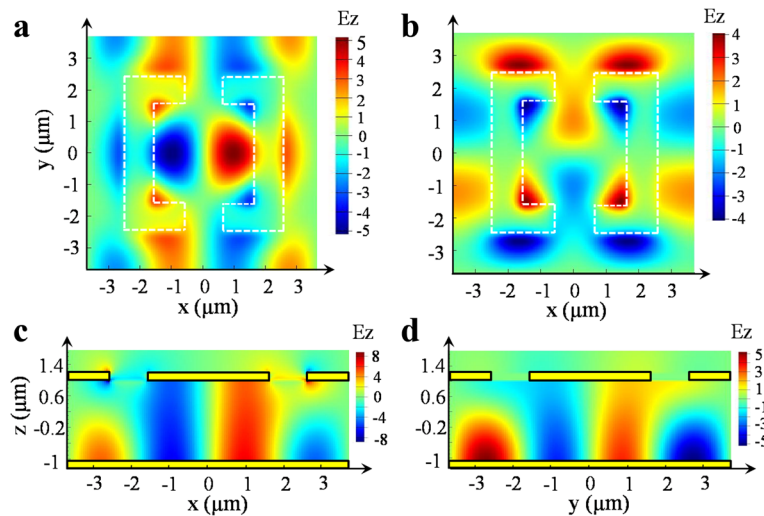


Fig. 3 FDTD-simulated E_z electric field component distributions for the device. (a), (b) E_z electric component distribution in x - y plane 200 nm below the metamaterial layer for E_x polarization at 10.7 μm (panel (a)) and E_y polarization at 10.3 μm (panel (b)), respectively. (c), (d) E_z electric component distribution in x - z and y - z planes at $y=0$ and $x=0$ for E_x polarization at 10.7 μm (panel (c)) and for E_y polarization at 10.3 μm (panel (d)), respectively

performed to remove the original InP substrate and reach the InGaAs etch stop layer. Next, $300 \times 400\text{-}\mu\text{m}^2$ device mesas are defined by standard photolithography and wet etching process. The mesa depth was controlled to reach the bottom reflection Au layer. Then $300 \times 300\text{-}\mu\text{m}^2$ CSRRs metamaterial areas and $300 \times 100\text{-}\mu\text{m}^2$ top electrodes were fabricated on the top of device mesas using a combination of standard photolithography and metal lift-off process. The CSRRs layer has a depth of 100 nm. The device fabrication was then completed with chip cleavage and gold wire bonding. In the top picture of Fig. 4, a large area scanning electron microscopy (SEM) image of the metamaterial integrated device is shown. The top and bottom electrical contacts are indicated in the figure. In the bottom picture of Fig. 4, the zoom-in views of the CSRRs are shown. The SEM images indicate that the morphology of CSRRs is not so idealized, which is limited to the method through which the CSRRs are obtained. However, this method is simple and of low cost and more promising for practical applications, such as fabricating large-area focal plane arrays.

Results and Discussion

Once the device processing is completed, it is mounted onto a copper heat-sink and then fixed on the cold finger of a liquid nitrogen cryostat for device response measurements. The photocurrent response measurement was performed by Nicolet 6700 fourier transform infrared spectrometer (FTIR) with a KBr beam splitter and the internal glow-bar illumination. With the measured photocurrent spectrum, the responsivity spectrums were calibrated using a standard blackbody

source. Figure 5a shows the photocurrent responsivity spectra of the metamaterial integrated devices. Also shown is that of a 45° edge facet coupling device made from the same QCD wafer as the reference. In this integrated device, the expected detector response is a convolution of the intersubband transitions in detector's active region and the metamaterial resonances. Therefore, the response spectrum shape of the CSRRs coupled device is clearly modified compared to the 45° edge facet coupling device. In addition, significant response enhancements are obtained at metamaterial resonances for both polarizations, as is shown in the inset of Fig. 5a. And the largest response enhancement factor of 165% is gained at the wavelength of 11.5 μm for the E_x polarization, which is far away from the peak response of the original device. This may be due to the low absorption for the original device, which will leave more electrons on the ground state for the metamaterial coupled absorption [30]. However, the response enhancement is not obtained in the whole response spectrum, which can be attributed to the narrow-banded property of the metamaterial resonances. In addition, at the peak response wavelength, incident light cannot coupled to the absorption region of the QCD structure efficiently through metamaterial resonances and thus the enhancement did not occur near the peak wavelength. Thus, in order to acquire enhancement through the whole response spectrum, metamaterial structures with broad-banded resonances should be designed and integrated to the detector [31]. Figure 5a also indicates that E_x polarization have stronger enhancement than the E_y polarization. To reveal the physical reason, the z -dependences of the total $|E_z|$ amplitude are calculated,

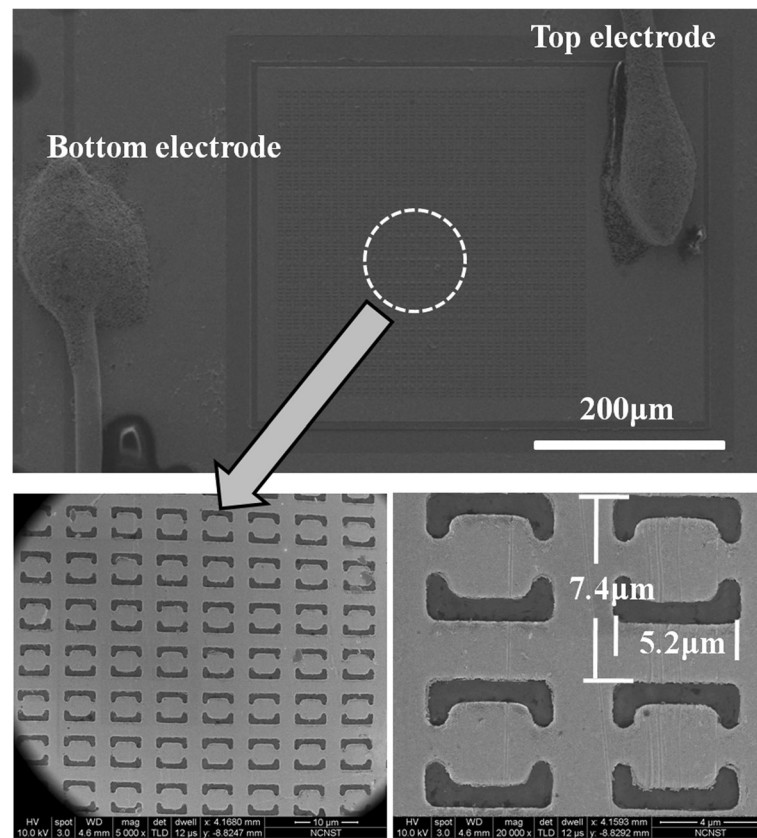
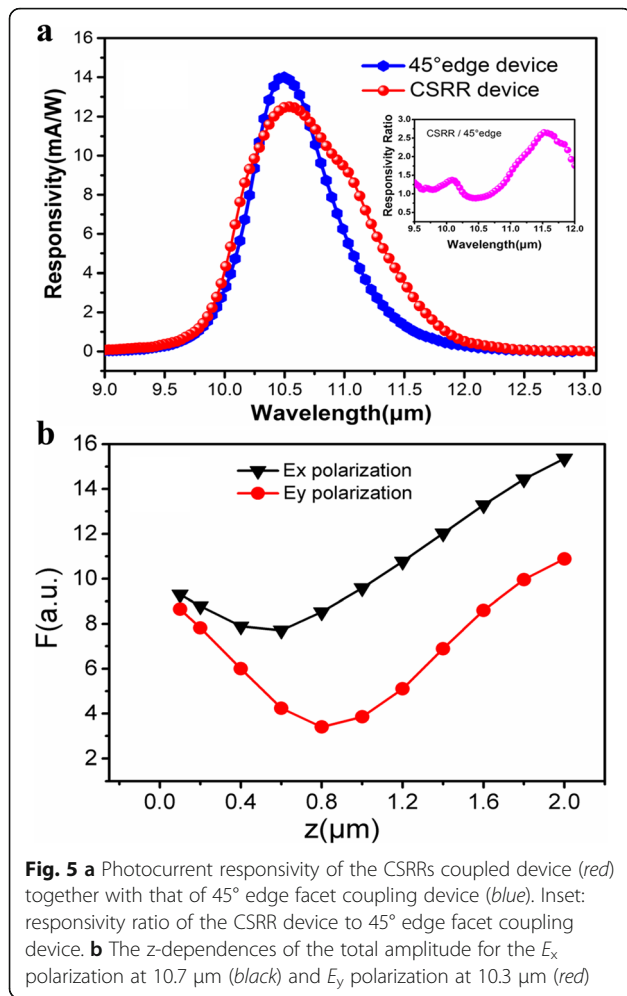


Fig. 4 Scanning electron microscopy images of the integrated device (*top*) and CSRRs structure (*bottom*)

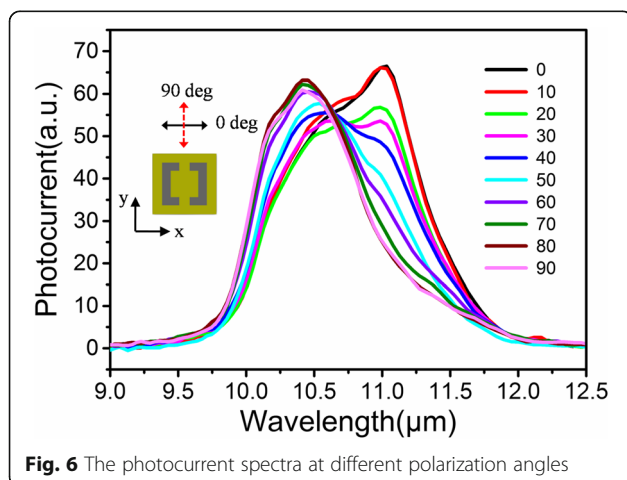
which is obtained by taking the areal integral $F = \left| \int_0^d \int_0^d |E_z(x, y)| dx dy \right|$, for both E_x and E_y polarization incident light at metamaterial resonances of 10.7 and 10.3 μm, respectively, and is demonstrated in Fig. 5b. The results clearly demonstrated that the $|E_z|$ areal integrals for E_x polarization incident light are larger than those for E_y polarization at different z positions. This indicates that E_x polarization incident light can excite E_z electric field more efficiently and thus bring in stronger response enhancement. Moreover, there are clear dips in F curves at the middle of the waveguide. Since the coupled modes are excited by the metamaterial layer and confined by the double-metal waveguide, it is expected that the E_z -field is strongest just underneath the top metal and close to the bottom metal contact. Due to the serial structure of QCD active region, the device responsivity will be limited by the region with small $|E_z|$ areal integral and thus low absorption. Therefore, further responsivity enhancement is in prospect by optimizing the position of absorption region in the waveguide, where the absorption region is layered at the positions with strongest E_z electric field. Another aspect that has to be considered is the ohmic losses due to the double-metal structure in the device, which will

absolutely reduce the coupled energy in the detector and thus limit the response enhancement. In order to obtain exciting responsivity enhancement through metamaterial couple, special designed structures with low ohmic losses need to be investigated and employed in further study [32].

To further gain the polarization-dependent property of the device, device photocurrent has been measured with different polarization incident light. Figure 6 is the photocurrent curves changing with the azimuth positions of the polarizer. 0° polarization corresponds to polarization in x direction and 90° in y direction, as is shown in the inset in Fig. 6. The results unambiguously show that the spectral responses are highly dependent on the incidence light polarization, which indicates the feasibility to design polarization-selective detectors using metamaterial resonances. However, the E_x/E_y response ratio for this device is somewhat small. This can be due to the complex mutual effect of grating and metamaterial resonances, which is expected as the periodicity of the metamaterial is comparable to the effective wavelength inside the active region. In order to obtain high polarization discriminating detectors for practical application, such as polarimetric imaging, optimized metamaterial design should be implemented [33].



Furthermore, taking advantage of the unique properties of metamaterial, various metamaterial designs can be employed to implement multi-functional detector. For example, metamaterial structures with chirality can be applied to fabricate circular polarization discriminating detectors [34].



Conclusions

In conclusion, a polarization-dependent normal incident quantum cascade detector coupled via complementary split-ring metamaterial resonators has been demonstrated. The metamaterial structure is fabricated directly into the top metal contact and forms a double-metal waveguide together with the metallic ground plane. With normal incidence, significant enhancements of photocurrent response are obtained at the metamaterial resonances compared with the 45° edge facet coupling device. And the largest response enhancement factor of 165% is gained at the wavelength of 11.5 μm for the E_x polarization. The response spectral also exhibits clearly polarization dependence, which outlines the advantages of metamaterial coupled design for polarization discriminating application. In further, taking advantage of the unique properties of metamaterial, many new IR detector functionalities can be implemented by designing suitable metamaterial structures, which presents a promising way for fabrication of high performance or special functional device for practical applications.

Abbreviations

CSRR: Complementary split-ring resonator; FDTD: Three-dimensional finite-difference time-domain; FTIR: Fourier transform infrared spectrometer; QCDs: Quantum cascade detectors; SEM: Scanning electron microscopy; SL: Superlattice

Acknowledgements

The authors would like to thank Ping Liang and Ying Hu for their help in device processing.

Funding

This work was supported by the National Natural Science Foundation of China (Grant Nos. 61504135, 61376051) and the National Basic Research Program of China (Grant No. 2013CB632804/02).

Authors' contributions

LW have provided this idea, designed the structure, doing most of the simulation and wrote part of the paper. S-QZ fabricated the device, performed the testing, and wrote part of the paper. F-JW performed part of the device measurement. J-QL and F-QL revised the paper and supervised the project. S-ML and LJ Wang gave some helpful discussions on the device measurement. NZ completed the MBE growth of the wafer. ZGW supervised the project. All authors read and approved the final manuscript.

Competing interests

The authors declare that they have no competing interests.

Received: 22 September 2016 Accepted: 21 November 2016

Published online: 01 December 2016

References

- Rogalski A, Antoszewski J, Faraone L (2009) Third-generation infrared photodetector arrays. *J Appl Phys* 105:091101
- Levine BF (1993) Quantumwell infrared photodetectors. *J Appl Phys* 74:R1–R81
- Liu HC, Jianmeng L, Buchanan M, Wasilewski ZR (1996) High-frequency quantum- II infrared photodetectors measured by microwave-rectification technique. *IEEE J Quantum Electron* 32:1024–1028
- Gendron L, Carras M, Huynh A, Ortiz V (2004) Quantum cascade photodetector. *Appl Phys Lett* 85:2824–2826
- Giorgetta FR, Baumann E, Graf M, Yang Q, Manz C, Köhler K, Beere HE, Ritchie DA, Linfield E, Davies AG, Fedoryshyn Y, Jäckel H, Fischer M, Faist J, Hofstetter D (2009) Quantum cascade detectors. *IEEE J Quantum Electron* 45:1039–1052

6. Giorgetta FR, Baumann E, Théron R, Pellaton ML, Hofstetter D, Fischer M, Faist J (2008) Short wavelength 4 μm quantum cascade detector based on strain compensated InGaAs/InAlAs. *Appl Phys Lett* 92:121101
7. Vardi A, Bahir G, Guillot F, Bougerol C, Monroy E, Schacham SE, Tchernycheva M, Julien FH (2008) Near infrared quantum cascade detector in GaN/AlGaIn/AlN heterostructures. *Appl Phys Lett* 92:011112
8. Giorgetta FR, Baumann E, Hofstetter D, Manz C, Yang Q, Köhler K, Graf M (2007) InGaAs/AlAsSb quantum cascade detectors operating in the near infrared. *Appl Phys Lett* 91:111115
9. Graf M, Hoyler N, Giovannini M, Faist J, Hofstetter D (2006) InP-based quantum cascade detectors in the mid-infrared. *Appl Phys Lett* 88:241118
10. Kong N, Liu JQ, Lu L, Liu FQ, Wang LJ, Wang ZG, Lu W (2010) A 10.7 μm InGaAs/InAlAs quantum cascade detector. *Chin Phys Lett* 27:128503
11. Buffaz A, Carras M, Doyennette L, Nedelcu A, Marcadet X, Berger V (2010) Quantum cascade detectors for very long wave infrared detection. *Appl Phys Lett* 96:172101
12. Giorgetta FR, Baumann E, Graf M, Ajili L, Hoyler N, Giovannini M, Faist J, Hofstetter D, Krötz P, Sonnabend G (2007) 16.5 μm quantum cascade detector using miniband transport. *Appl Phys Lett* 90:231111
13. Zhai SQ, Liu J-Q, Wang XJ, Zhuo N, Liu FQ, Wang ZG, Liu XH, Li N, Lu W (2013) 19 μm quantum cascade infrared photodetectors. *Appl Phys Lett* 102:191120
14. Graf M, Scalari G, Hofstetter D, Faist J (2004) Terahertz range quantum well infrared photodetector. *Appl Phys Lett* 84:475–477
15. Reininger P, Schwarz B, Detz H, Farland DM, Zederbauer T, Andrews AM, Schrenk W, Baumgartner O, Kosina H, Strasser G (2014) Diagonal-transition quantum cascade detector. *Appl Phys Lett* 105:091108
16. Reininger P, Schwarz B, Gansch R, Detz H, MacFarland D, Zederbauer T, Andrews AM, Schrenk W, Strasser G (2015) *Opt Express* 23:6283–6291
17. Hinds S, Buchanan M, Dudek R, Haffouz S, Laframboise S, Wasilewski Z, Liu HC (2011) Near-room-temperature mid-infrared quantum well photodetector. *Adv Mater* 23:5536–5539
18. Wang XJ, Liu JQ, Zhai SQ, Liu FQ, Wang ZG (2014) Room temperature quantum cascade detector operating at 4.3 μm . *J Semiconductors* 35:104009
19. Harrer A, Schwarz B, Schuler S, Reininger P, Wirthmüller A, Detz H, MacFarland D, Zederbauer T, Andrews AM, Rothermund M, Oppermann H, Schrenk W, Strasser G (2016) 4.3 μm quantum cascade detector in pixel configuration. *Opt Express* 24:17041–17049
20. Wang YC, Li SS (1994) Design of a two-dimensional square mesh metal grating coupler for a miniband transport GaAs quantum-well infrared photodetector. *J Appl Phys* 75:582–587
21. Zhai SQ, Liu JQ, Liu FQ, Wang ZG (2012) A normal incident quantum cascade detector enhanced by surface plasmons. *Appl Phys Lett* 100:181104
22. Reininger P, Schwarz B, Harrer A, Zederbauer T, Detz H, Andrews AM, Gansch R, Schrenk W, Strasser G (2013) Photonic crystal slab quantum cascade detector. *Appl Phys Lett* 103:241103
23. Chen T, Li S, Sun H (2012) Metamaterials application in sensing. *Sensors* 12: 2742–2765
24. Pendry JB, Holden AJ, Robbins DJ, Stewart WJ (1999) Magnetism from conductors and enhanced nonlinear phenomena. *IEEE Trans Microw Theory Tech* 47:2075–2084
25. Shelby RA, Smith DR, Schultz S (2001) Experimental verification of a negative index of refraction. *Science* 292:77–79
26. Dayal G, Ramakrishna SA (2014) Design of highly absorbing metamaterials for infrared frequencies. *Opt Express* 20:17503–17508
27. Liu XL, Starr T, Starr AF, Padilla WJ (2010) Infrared spatial and frequency selective metamaterial with near-unity absorbance. *Phys Rev Lett* 104:207403
28. Benz A, Campione S, Liu S, Montano I, Klem JF, Allerman A, Wendt JR, Sinclair MB, Capolino F, Brener I (2013) Strong coupling in the sub-wavelength limit using metamaterial nanocavities. *Nat Commun* 4:2882
29. Benz A, Krall M, Schwarz S, Dietze D, Detz H, Andrews AM, Schrenk W, Strasser G, Unterrainer K (2014) Resonant metamaterial detectors based on THz quantum-cascade structures. *Sci Rep* 4:4269
30. Kalchmair S, Detz H, Cole GD, Andrews AM, Klang P, Nobile M, Gansch R, Ostermaier C, Schrenk W, Strasser G (2011) Photonic crystal slab quantum well infrared photodetector. *Appl Phys Lett* 98:011105
31. Wu C, Shvets G (2012) Design of metamaterial surfaces with broadband absorbance. *Opt Lett* 37:308–310
32. Vora A, Gwamuri J, Pala N, Kulkarni A, Pearce JM, Guney D (2014) Exchanging ohmic losses in metamaterial absorbers with useful optical absorption for photovoltaics. *Sci Rep* 4:4901
33. Li Q, Li ZF, Li N, Chen XS, Chen PP, Shen XC, Lu W (2014) High-polarization-discriminating infrared detection using a single quantum well sandwiched in plasmonic micro-cavity. *Sci Rep* 4:6362
34. Li W, Coppens ZJ, Besteiro LV, Wang WY, Govorov AO, Valentine J (2015) Circularly polarized light detection with hot electrons in chiral plasmonic metamaterials. *Nat Commun* 6:8379

Submit your manuscript to a SpringerOpen[®] journal and benefit from:

- Convenient online submission
- Rigorous peer review
- Immediate publication on acceptance
- Open access: articles freely available online
- High visibility within the field
- Retaining the copyright to your article

Submit your next manuscript at ► springeropen.com